Research Article GU J Sci 35(): x-x (2022) DOI: 10.35378/gujs.912709

Gazi University

Journal of Science

http://dergipark.gov.tr/gujs

Effects of Cobalt Doping on the Structural, Optical, and Electrical Properties of SnO_2 Nanostructures Synthesized by SILAR Method

Muhammed Emin GULDUREN[1,*], Ahmet TASER[2], Harun GUNEY[3]

[1]*Agri Ibrahim Cecen University, Vocational School Department of Electric and Energy, 04200, Agri, Turkey*
[2]*Agri Ibrahim Cecen University, Patnos Vocational School, Department of Medical Services and Techniques, Agri, Turkey*
[3]*Ataturk University, Hinis Vocational School, Department of Medical Services and Techniques, Erzurum, Turkey*

Highlights

- Cobalt doping into SnO_2 samples grown successfully by SILAR method.
- The bandgap of SnO_2 was red-shifted due to Co doping.
- The PL emission intensity can be controlled by cobalt content in the SnO_2 lattice.
- Co ions were efficiently incorporated into host SnO_2 structure.
- Semiconductor nature of samples was reported in the electrical characterization.

Article Info

Received: 10 April 2021
Accepted: 26 Aug 2021

Keywords

Co:SnO_2 thin films
SILAR
XRD
Bandgap
PL

Abstract

Undoped and cobalt (Co) doped tin oxide (SnO_2) films were prepared onto glass slides via the successive ionic layer adsorption and reaction (SILAR). Variable characterization methods were applied to examine the effects of cobalt impurities on physical properties of SnO_2 films. The performed characterization measurements were X-ray diffraction, Ultraviolet–visible spectrometer, Photoluminescence, and Raman. No peak ascribed to Co, SnO, or Sn was found in the XRD spectrum which may indicate the integration of cobalt in SnO_2 crystal lattices. And the obtained XRD peaks may be related to the tetragonal rutile phase of pure SnO_2. SEM images exposed that the Co dopant atoms affectedthe sample morphologies. The optical analyses showed that the transmittance and reflectance percentages dropped by the introduction of impurities to the SnO_2 system as the absorbance values of doped SnO_2 samples increased. Thus,a red shift (2.6–1.8 eV) occurred in the bandgapsas Co concentration changed in the films. The Raman spectra of pure SnO_2 and Co:SnO_2 samples exhibited major peaksaround 481 cm^{-1}, 571 cm^{-1} and 602 cm^{-1}. In photoluminescence spectrum, it was noted that the emission intensity can both increase or decrease due to the different cobalt doping ratios in the SnO_2 nanostructures. Resistance measurements displayed that the resistivity increased with the increment of doping concentration. However, it was shown that the electrical conductivities could be increased after the heat treatment of glass substrates up to 500 ^oC, a common behavior of semiconductor materials.

EARLY VIEW

1. INTRODUCTION

Recently, metal oxide semiconductors (MOSs) like CdO, ZnO, SnO_2, CuO, In_2O_3 and TiO_2 have received considerable attention due to their wide-ranging applications like LEDs, solar cells, gas sensors, display panels, transparent electrodes and so forth [1, 2]. SnO_2 is a well-recognized unique n-type semiconductor due to its intriguing electrical and optical properties. SnO_2 thin films are highly conductive and transparent in the visible spectrum with direct bandgap energy of 3.67 eV [3]. And, by being a wide bandgap nanomaterial, it is an excellent candidate to be employed in optoelectronics. However, most of the previous studies on MOSs focused on zinc oxide (binding energy=60 meV, bandgap=3.37 eV) [1, 4]. Hence, there is a gap in the literature on characterizing SnO_2 thin films produced by different methods. Besides, it is noted that SnO_2 nanostructures have a wider bandgap including a higher binding energy (130 meV) which may help enhancing the performance of the blue emission devices which are based on tin oxides [5, 6].

One important method to accomplish better physical characteristic features of SnO_2 films is to modify the traits of these semiconductor nanostructures by the introduction of transition metal dopants (Cr, Co, Fe, Ni,

*Corresponding author, e-mail: megulduren@agri.edu.tr

Mn, Zn, etc.) into the parent system [3, 6-8]. For example, the photoluminescence emission intensity and bandgap energy of SnO_2 thin films, which can be significant factors that decide their successes in the optoelectronic applications, have been shown to be affected due to the presence of dopants in their crystal system [5, 6, 8]. Among the dopant elements, the studies related to the incorporation of cobalt (Co; [Ar] $3d^7 4s^2$) into the SnO_2 lattices (SCO) are incomplete, even though cobalt has a broad branch of utilizations in batteries, catalysis and electroplating [9]. Moreover, researchers have carried out considerable amount of work on the sensors and catalysts features of tin oxide samples, however, optical traits of SnO_2 were studied less compared to other oxide nanostructures. Therefore, researches on the optical characters of SnO_2 nanoparticles would be very valuable for the related science fields. There are several numbers of methods that are available to synthesize SnO_2 nanocrystallites like pulsed laser deposition (PLD), sol–gel, spray pyrolysis, magnetron sputtering, hydrothermal routes, spin coating, chemical vapor deposition, etc. [5-12]. In the present investigation, we have adapted the SILAR method for the preparation of cobalt doped SnO_2 ($Co:SnO_2$) nanoparticles as this method is easily operated with no sophisticated equipment.

Although, a large number of studies have been carried out on the SnO_2 semiconductor nanostructures, the investigations of the Co doped SnO_2 nanoparticles appear to be inadequate, all things considered. Based on the literature survey, to find a complete work regarding the influence of Co impurity on the physical properties of SnO_2 thin films is very limited. Therefore, more studies should be conducted on the cobalt doped SnO_2 nanostructures to comprehend the impacts of the introduced impurities into the SnO_2 crystal lattice. Currently, in the web of science database, there are 19 studies which include "cobalt doped tin oxide" as keywords in their title. Additionally, no results appear if "SILAR" term is included to this search in the same database. As a new approach, we have prepared pure SnO_2 and $Co:SnO_2$ thin films by employing the SILAR deposition method. Also, the influence of Co doping on the structural, morphological, optical and electrical properties of SnO_2 thin films is investigated by using the XRD, FESEM, Uv-vis spectrometer, Raman, Photoluminescence and two probe resistance vs temperature measurements. Here, in this article we present the synthesis and characterization of undoped SnO_2 and $Co:SnO_2$ thin films grown by the SILAR technique which requires neither expensive equipments nor a complex system. And, we believe that this will be the first work that performed the SILAR deposition to fabricate cobalt doped SnO_2 nanostructures.

2. MATERIAL METHOD

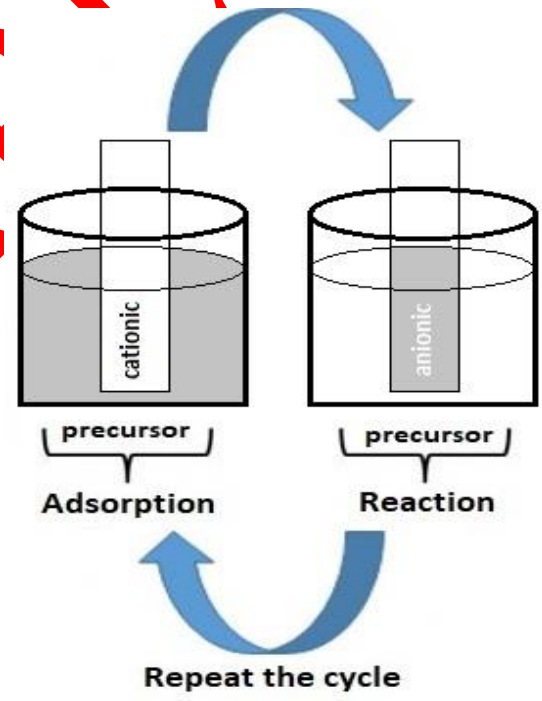


Figure 1. *One cycle of SILAR deposition method*

EARLY VIEW

Undoped and Co doped SnO_2 nanostructures have been produced by the SILAR method onto the glass slides. Detailed growth process of thin films was described in our previous studies [13]. However, in this study, cationic precursor for pure SnO_2 (SCO) sample was prepared using 0.1 molar (M) tin chloride ($SnCl_2$ + 6H2O). And, 0.1 M cobalt chloride ($CoCl_2$) were used as doping agent at different ratios, 0.5%, 1%, 2%, and 4% which were named as SCO1, SCO2, SCO3, and SCO4, respectively. Total of 70 cycles were performed for this particular set of experiment as one cycle shown in Figure 1. Afterwards, the thin films were dried in open air, and later placed in a convection ashing furnace for an hour at 400 °C.

3. THE RESEARCH FINDINGS AND DISCUSSION

The XRD spectra of the undoped SnO_2 and Co:SnO_2 thin films are displayed in Figure 2. The maindiffraction peak positions (°2θ) at 26.65º, 34º, 38º, and 51.9º of all samples are assigned to the tetragonal, rutile SnO_2 of polycrystalline nanostructures (ICDD card No. 77-0452), and the diffraction peaks can be indexed to (110), (101), (200) and (211) lattice planes, respectively. Neither any other impurity peaks nor any significant shifts in the XRD spectra for Co, SnO or Sn was detected in the XRD pattern which may indicate that annealing the thin films at 400 ºC was a suitable temperature to obtain fully oxidized SnO_2 nanostructures [11]. Also, this formation can be interpreted as the evidence of homogeneously scattered of Co into the SnO_2 matrix as the radii difference between Co^{2+} (0.65 Å) and Sn^{4+} (0.69 Å) is negligibly small so that Co^{2+} can substitute Sn^{4+} in the crystal system which is compatiblewith previous reports [14, 15]. Table 1 presents the crystalline size *(D)*, dislocation density *(δ)* and lattice strain *(ε)* of all the samples, computed by the performing formulas below [3, 5-8]

$$D=\frac{0{,}9\lambda}{\beta\ cos\theta} \quad (1)$$

$$\delta=\frac{1}{D^2} \quad (2)$$

$$\varepsilon=\frac{\beta\ cos\theta}{4} \quad (3)$$

where λ is the wavelength of X-ray radiation, and β is the full width at half maximum (FWHM) of the peaks at the Bragg diffraction angle θ in degree. The intensity of XRD peaks decreased and FWHM increased due to strengthened Co presence as shown in the Figure 2 and Table 1, which were originated from the deformities in the crystallites. This incidence may suggest that, although the Co^{2+} atoms take up the space which meant for Sn^{4+} elements, they generate defect sites in the crystals around the dopants. Also, this will ignite a chain reaction, and eventually affect the charge densities of these semiconductor nanomaterials. Table 1 and Figure 3 (f) revealed that the calculated crystalline size (*D*) of SnO_2 nanostructures showed increment for the lower cobalt doping ratios, but then the *D* values dropped down as Co^{2+} ions multiplied. This data may hint that the increasing Co^{2+} ions in SnO_2 lattice and annealing thin films may have a tendency of both enhancing and blocking effects on the growth of crystal grains. Accordingly, the formation of smaller crystals may be caused by the improved density of nucleation centers which belongs to the 2% and 4% Co doped SnO_2 thin films [3, 7, 11].

The variations in the lattice parameter (*a*) and interplanar distances (*d*) for the tetragonal rutile SnO_2 phases are also computed for different doping rates, and their values are tabulated in Table 1 as well. And, these values are compatible with the JCPDS card No. 72-1147. The values of *a* increase or decrease with varying densities of Co ions in the SnO_2 lattice in a random manner. This change in *a* may suggest that the grains of these thin films are constrained due to the cobalt doping and substitution of Co^{2+} and Sn^{4+} ions in the crystal system as they own comparable ionic radiuses. Furthermore, decreasing lattice parameters may imply that Co ions are well incorporated into the SnO_2 nanostructures [7, 10].

The microstrain and dislocation density were observed to be increased as a result of increase in cobalt doping concentrations to the 2% and 4%, unlike the same values recorded for the lower doping concentration levels. The crystallization process in polycrystalline nanostructures may ignite the change in microstrain and dislocation density due to the differences in the ionic sizes of Co^{2+} and Sn^{4+}materials [5,

EARLY VIEW

16]. Therefore, it is safe to say that there is a clear relation between crystallite size, microstrain, dislocation density, and cobalt doping. Moreover, the variation in crystallite size, dislocation density and microstrain may point out the formation of improved or weakened crystal structure, due to the cobalt doping [5-7].

Table 1. *Peak positions (^{0}2θ), FWHM, inter-planer distance (d), the particle sizes (D), the dislocation density (δ), the microstrain (ε), and the lattice constant (a) values of the pure and Co doped SnO_2 thin films*

Sample name	Pos. (°2θ)	FWHM (°2θ)	*d*-spacing (Å)	*D* (nm)	δ (10^{13} cm^{-2})	ε (10^{-2} %)	*a* (Å)
SnO	26,55	0,714	3,355	20,84	23,03	0,17	4,7441
SCO1	26,65	0,591	3,342	25,18	15,77	0,14	4,7266
SCO2	26,59	0,696	3,350	21,38	21,88	0,17	4,7371
SCO3	26,71	0,998	3,335	14,91	44,96	0,24	4,7162
SCO4	26,50	0,733	3,361	20,30	24,27	0,18	4,7529

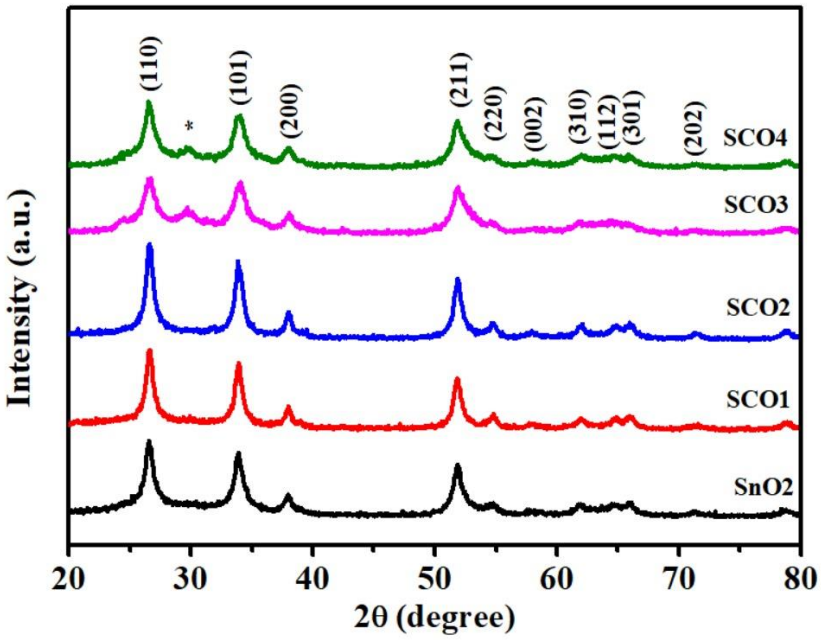


Figure 2. *XRD spectra of SILAR grown SnO_2 and Co:SnO_2 nanostructures*

Figure 3 shows the SEM morphologies of pure SnO_2 and SCO thin films. The pure and 1%, 2%, 4% Co doped SnO_2 nanostructures are magnified at 200 nm (see the Figure 3 (a), (c), (d), (e)), and 0.5% Co doped SnO_2 thin film is magnified at 300 nm as shown in the Figure 3 (b). Accumulations of irregular particle shapes can be seen in the Figure 3 from a to d while the SEM image for 4% cobalt doped SnO_2 thin film displays flowerlike structures as a result of the SILAR deposition process. Besides, it is observed that dense clusters are formed with the crystalline sizes in the range of 14 nm and 26 nm which is in agreement with our XRD analysis. Although, the Figure 3 (a) for pure SnO_2 thin film exhibits a less dense morphology with the voided grain boundaries, the clusters appear to be distributed more evenly in the related SEM figures (the Figure 3 (b), (c), (d)) as the cobalt doping concentration is increased from 0 to 2%. The semiconductor thin films with wider homogenous surface areas are considered to have the potential of reaching better optoelectronic device performances [17].

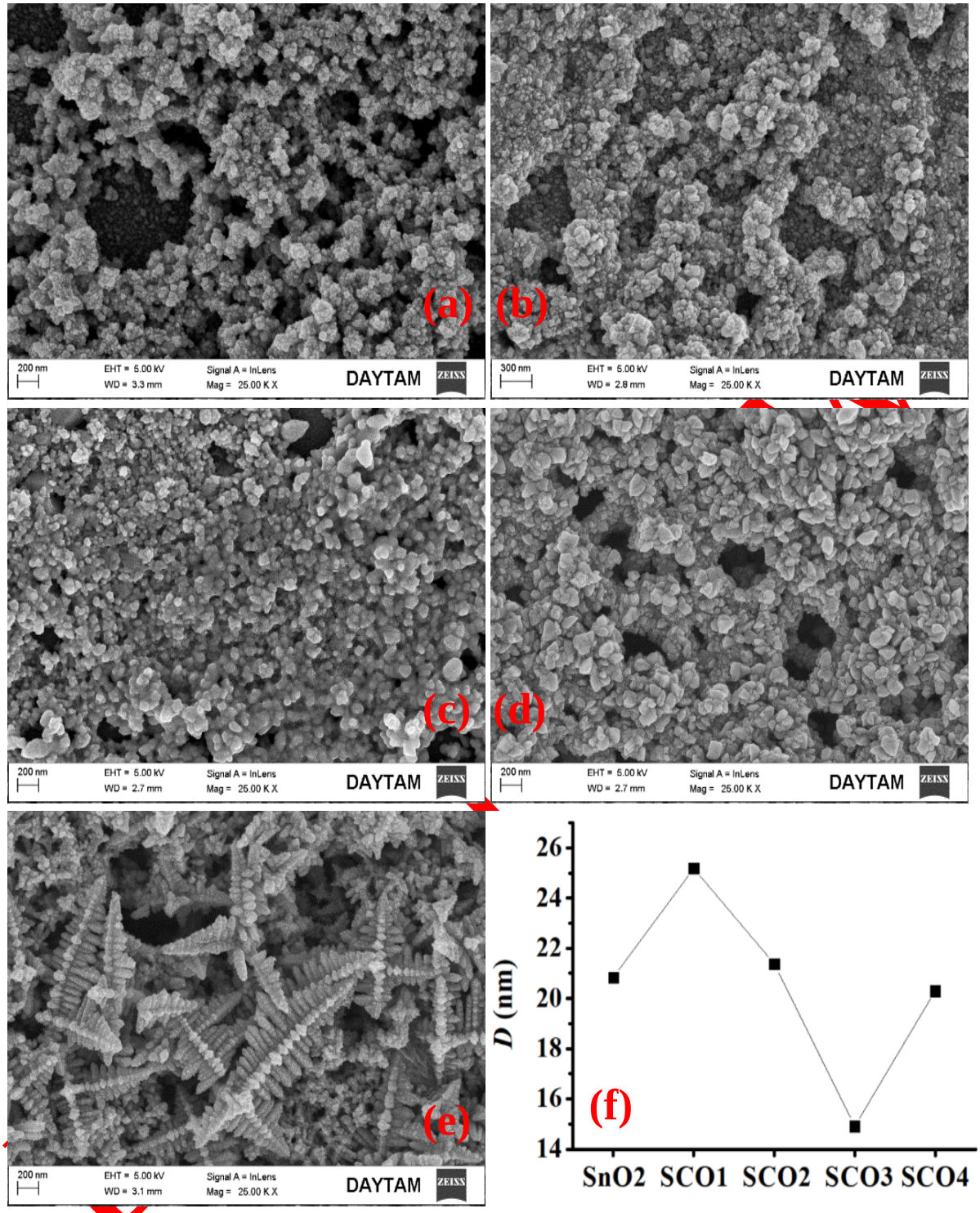


Figure 3. *FESEM images of pure (a) and Co (0.5%, 1%, 2%, and 4%) doped (b), (c), (d), (e) respectively, and crystallite sizes of undoped SnO_2 and SCO nanostructures (f)*

The optical absorption properties of pure SnO_2 and SCO thin films are shown in Figure 4. The absorbance spectrum of these nanostructures can be manipulated by many factors, for instance surface defects, bandgap, oxygen vacancies, and impurity centers. The obtained absorbance spectra, in the wavelength range of 300–1100 nm, unveils that the prepared samples went to an ultraviolet cut-off about 300 nm due to the excitations of electrons from valence band to conduction band. The absorption spectra of different samples clearly vary as the concentration of cobalt ions in the SnO_2 nanostructures was changed. And, it can be observed that the absorption decreases towards higher wavelenghts while it increases with the increased cobalt content in the thin films. The absorption spectrums, which are broadened as a result of the

change imourity levels in the produced SnO_2 nanocrystallites, may be attributed to the quantum confinement of the nanostructures [18].

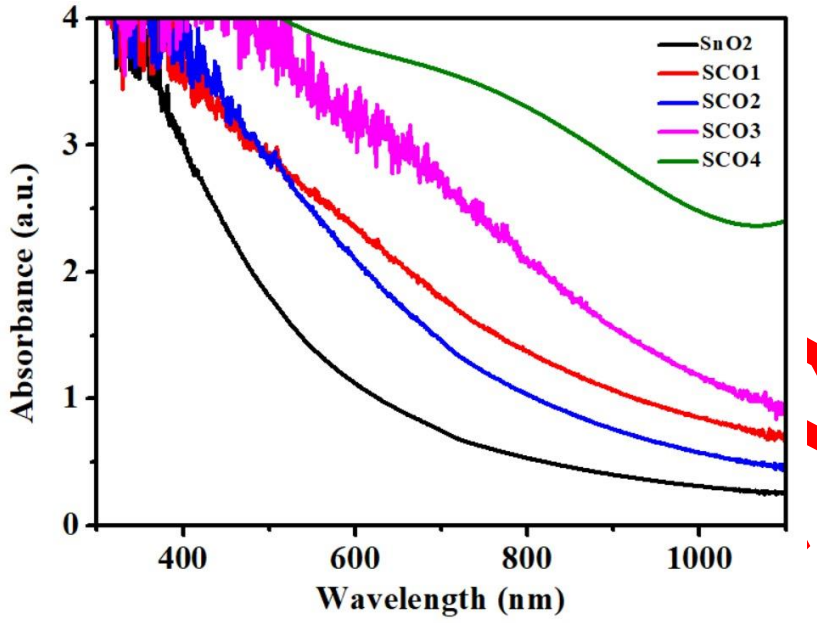


Figure 4. *The optical absorbance of SILAR grown SnO_2 and Co:SnO_2 nanostructures*

In Figure 5, the direct bandgap energies were calculated by applying the Tauc relation;

$$\alpha = \frac{Absorbance}{t} \tag{4}$$

$$(\alpha h\upsilon) = A\left(h\upsilon - E_g\right)^n \tag{5}$$

where $h\upsilon$ refers to the photon energy, A is an energy-independent constant semiconductor, t quantifies the thickness, and α symbolizes the absorption coefficient. The bandgap values was found to be 1.8 eV, 1.9 eV, 2.2 eV, 2.3 eV and 2.6 eV for 0.5%, 1%, 2%, 4% cobalt doped and pure SnO_2 nanostructures, respectively. Even though, the bandgap of bulk SnO_2 was reported to be 3.6 eV, the lowest theoretical bandgap of SnO_2 was found to be 0.6 eV with the presencce of impurities in SnO_2 crystals [19]. The bandgap energy decreases as a result of doping with cobalt ions as shown in the Figure 5. There are several explainations to this phenomenon. First of all, these narrowed bandgaps may be signs of the alloying effect of host material with varied cobalt dopants. Besides, this red shift in the bandgap of SCO thin films may also be activated by change in charge carrier density, oxygen vacancies, and the sp-d exchange interactions between Co^{2+} and Sn^{4+} ions. Also, as discussed in the XRD analysis and displayed in Table 1, the increasing cobalt doping ratio led to the sinking of grain boundaries, hence the enlargement of dislocation densities and microstrain, correspondingly. This may also result in bandgap narrowing [3, 5, 20-22]. Furthermore, it is noted that the found bandgap of SnO_2 samples are comparable with that of CdO thin films reported by Dugan et al and that of Co_3O_4 and NiO samples studied by Yetim et al, which are all promising metal oxides that can be used for optoelectronic applications [23, 24]. However, it is also possible to have different optical energy bandgaps for different needs as İlhan et al showed Cu_2NiSnS_4 having lower bandgap values than the SnO_2 nanostructures presented here [25].

Figure 6 displays the optical transmittance of pure SnO_2 and SCO thin films annealed at 400 ^oC for 1.0 h. The transmission characteristic is inversely proportional with absorption behavior as it is shown in the Figure 4. The pure SnO_2 thin film exhibits higher transparency for the inspected wavelength range as it is compared to the thin films where cobalt atoms integrated in. It is noted that the transmittance of the doped samples was considerably decreased as cobalt doping concentration increased from 0 to 4% as shown in the Figure 6. This result was also reported by other researchers in the previous studies [22, 26]. The lowered

EARLY VIEW

transmittance percentages may acknowledge the crystal defects which are generated as a result of cobalt dopants introduced to the system, and these defects prevents the scattering of lights. Besides, the shrinking of crystallite sizes due to cobalt dopingcan lead to the occurrence of weakened transmission values for doped SnO_2 nanostructures [3, 11, 27].

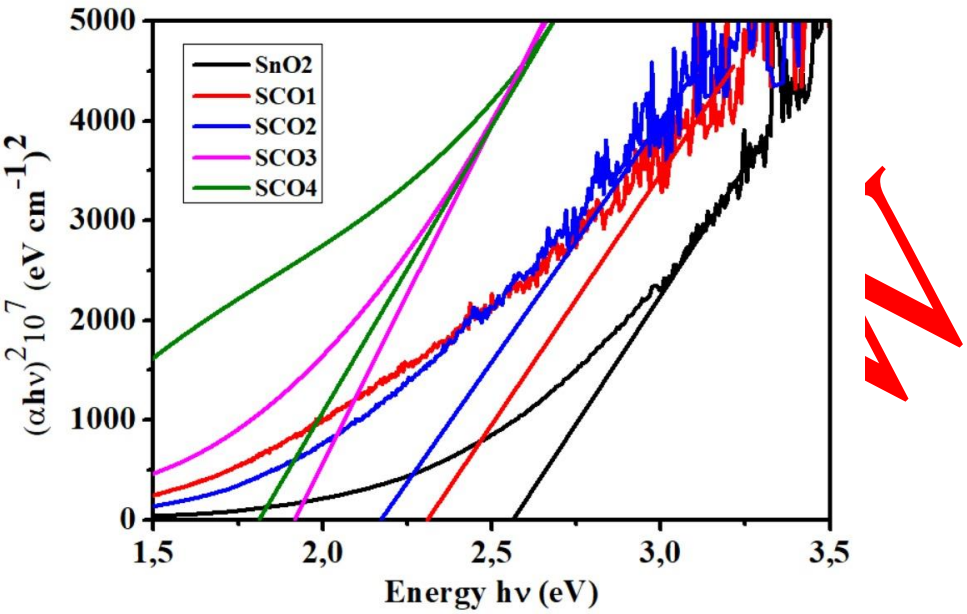


Figure 5. *The variation in E_g of SILAR grown SnO_2 and Co:SnO_2 nanostructures*

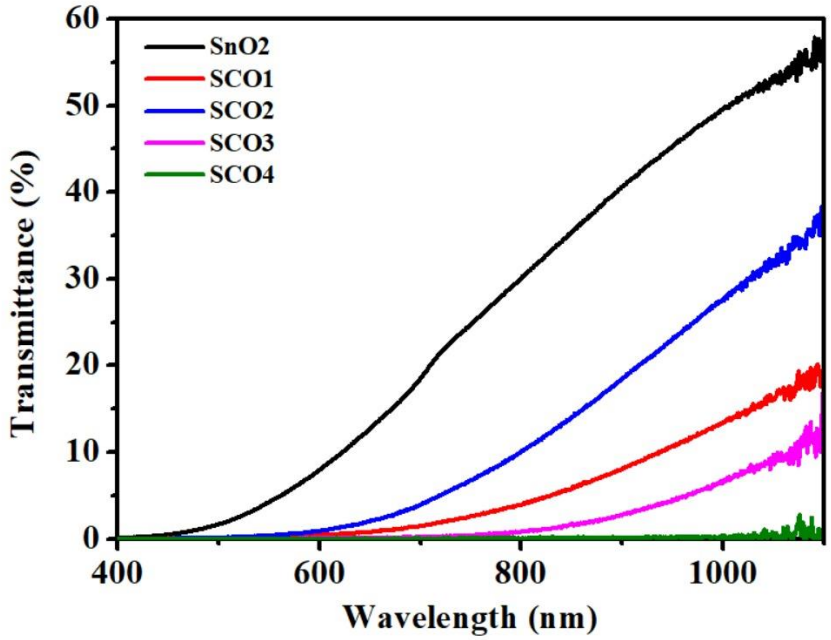


Figure 6. *The optical transmittance of SILAR grown SnO_2 and Co:SnO_2 samples*

Figure 7 shows the optical reflectance measurement which was conducted by UV-Vis spectrometer. The reflectance spectra of all samples start from zero percentage as this point in the spectrum corresponds to absorption edge shown in the Figure 4. The pure sample demonstrates varying reflectance percentages between 400 nm to 1100 nm, and the highest reflectance in this spectrum range was detected around 60% in the electromagnetic spectra of NIR. On the other hand, the reflectance of SCO samples decreased as cobalt doping concentration increased, and eventually almost vanished as seen in the Figure 7. The decrement in the reflectance may be explained by the surface imperfections which formed by the impurities

which increased the in-gap absorption and decreased internal reflection of pure SnO_2 nanocrystallites [22, 26].

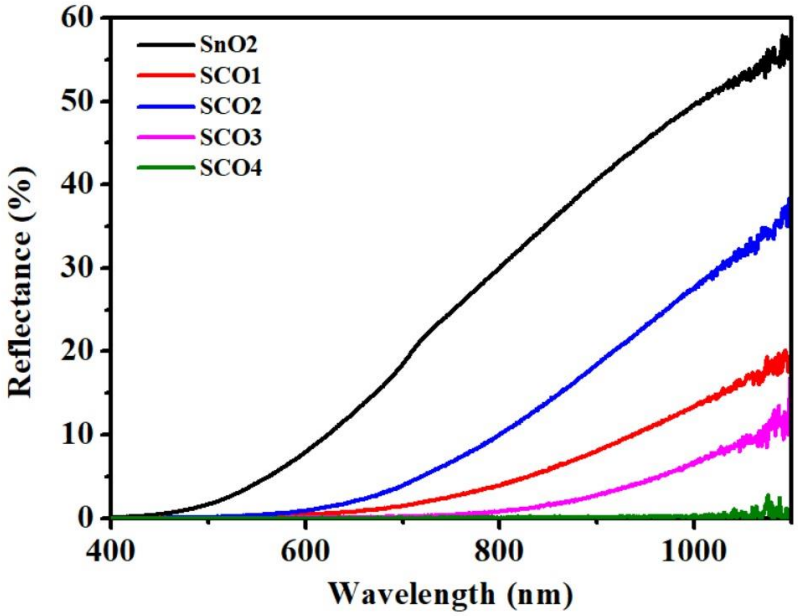


Figure 7. *The optical reflection patterns of SILAR grown SnO_2 and Co:SnO_2 nanostructures*

In Figure 8, the photoluminescence emission intensities are illustrated for the pure SnO_2 and SCO nanostructures prepared by SILAR technique. The PL spectrum helps to gather valuable information on the deformations of the produced SnO_2 nanostructures which originated from cobalt doping atoms in the crystal system. The PL emission curves of pure and 0.5%, 1% cobalt doped SnO_2 thin films show two main emission peaks in the visible spectrum which are centered at 416 nm (2.98 eV) and 551 nm (2.25 eV). It is clear that thefirst two doping levels of cobalt increased the PL emission intensity. However, the higher Co doping ratios decreased the intensity and combined the two main peaks into one which was centered at 551 nm. Also, a shoulder peak for 2% and 4% cobalt doped SnO_2 samples were occurred in the PL spectrum which was located at 652 nm(1.90 eV). The obtained peaks can be attributed to violet, green, and red emission bands, respectively. In addition to that, it is well known that oxygen deficiencies are one of the decisive factors on tuning the PL emission intensity. The weakened emission intensities may point out the electron-hole pair recombinations, created by oxygen vacancies, which ultimately may cause the higher photocatalytic activity to occur as a result. And, these changes in the emission intensities can also be related to the red shift in the optical band gap which was proven by XRD and Uv-vis analysis [7, 11, 28, 29].

The Raman measurements of the pure SnO_2 and SCO samples grown by SILAR technique were shown in Figure 9 so that it enables to further prove the presence of cobalt dopant related distortionsin the SnO_2 crystallites which results in the vibrational modes [5]. The Raman spectra of the pure SnO_2 and SCO2, SCO3 and SCO4 crystal structures display two distinct peaks centered at around 481 ± 2, and 602 ± 2 cm^{-1}. However, it is observed that the SCO1 thin film shows only one noticeable peak, located at $571cm^{-1}$. Therefore, these peaks could be ascribed to E_g, S_2 (surface phonon mode) and A_{1g} fundamental modes of tetragonal rutile SnO_2 [30]. The Figure 9 also reveals that the intensity of these modes for the samples with different doping concentrations has either showed small changes or diminished with varied doping ratios which affirms the successful incorporation of cobalt ions into SnO_2 lattice. Moreover, the variations in the measured Raman spectra can be related to the altered structural features of the tin oxides samples due to the introduced impurities to the SnO_2 nanostructures, which is supported by the XRD results [5, 30].

EARLY VIEW

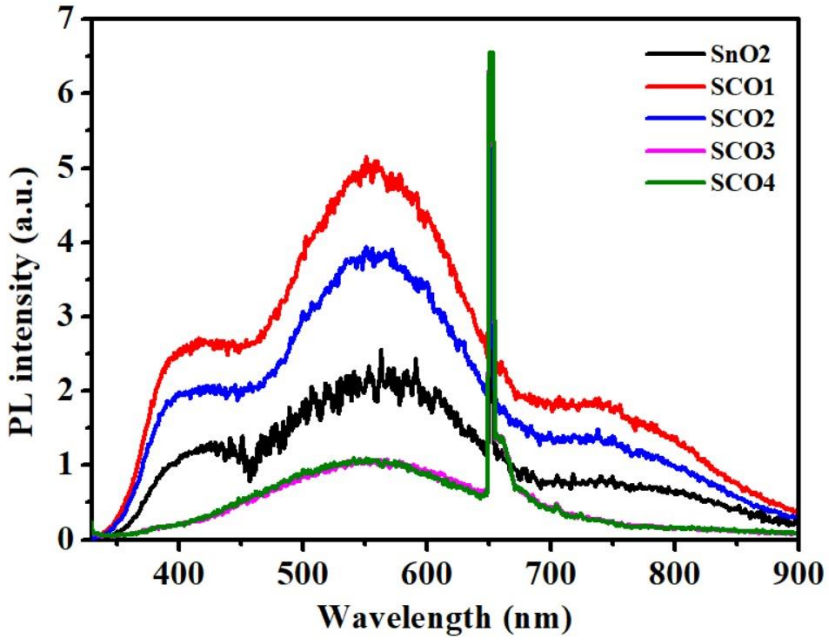


Figure 8. *The PL emission patterns of SILAR grown SnO_2 and Co:SnO_2 nanostructures*

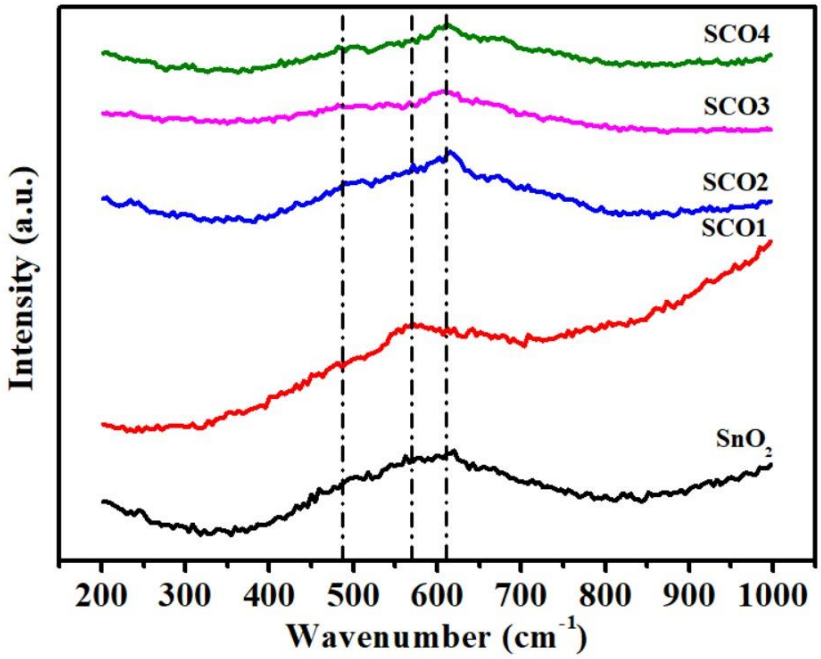


Figure 9. *Raman spectrum of SILAR grown SnO_2 and Co:SnO_2 nanostructures*

In Figure 10, the variation in the resistance for the pure SnO_2 and SCO thin films depending on substrate temperature have been evaluated in an attempt to have an idea on the electrical properties of the prepared SnO_2 nanostructures. The Figure 10 uncovered that the resistivity decreased while the temperature increased from 50 to 500 ^{0}C, which is in good agreement with the literature [11]. This behavior may be originated from thermally activated charge carriers and their mobility. The resistance was high at low temperatures, however, it reduced with the increment in temperature. On the contrary, the resistance slightly increased again owing to the fact that the elimination of oxygen vacancies after 300 ^{0}C. In general, the charge carriers of a material is inversely proportioned with its resistance, thus lower resistance with enhanced carrier concentration will encourage better electrical conductivity results. Also, there are other factors that may affect the efficiency of charge carriers such as crystallinity, grain size, surface contact areas, etc. [3, 10, 11].

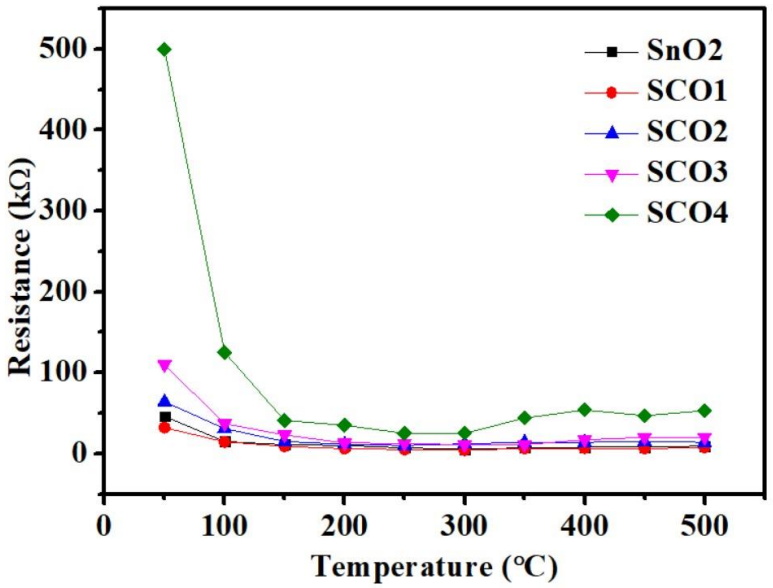


Figure 10. *Change in resistance of SILAR grown SnO_2 and Co:SnO_2 nanostructures with respect to temperature*

4. CONCLUSIONS

All in all, SILAR grown pure SnO_2 and Co:SnO_2 thin films have been obtained onthe glass slides at room temperature. Structural analysis concluded that the pure SnO_2 and Co:SnO_2 nanostructures have the rutile tetragonal phase of polycrystalline SnO_2. The surface morphologies of the prepared SnO_2 samples were noticeably modified where the random shaped and flowerlike crystals formed due to the deposition method and cobalt dopants. The resistivity of the analyzed samples was increased due to the increment in the cobalt subjects whereas the electrical conductivity was inversely proportioned, which is considered as characteristic trait of semiconductors in the presence of varying temperature. The optical evaluations concluded that the bandgaps of films red shifted simultaneously with the increased concentration of cobalt ions in SnO_2 nanostructures. This change in bandgap may be caused by the presence of increased deformations in the Co:SnO_2 crystals, such as modified grain sizes, dislocation densities, microstrain, and oxygen vacancies. Furthermore, the transmittance and reflectance in the visible region decreased while the absorbance values showed opposite trend as Co content increased. The PL spectrum of produced SnO_2 nanostructures showed both increment and decrement in the emission intensities which may also be caused by the defects in the SnO_2 nanocrystallites formed by cobalt contents. Therefore, it is safe to say that the physical aspects of SnO_2 can be modulated by forming defects with different doping ratios in the grown SnO_2 crystallites. Accordingly, this can aiddevelopingnew materials to be used in catalysis, optoelectronics, solar cells, LCDs and sensor applications.

ACKNOWLEDGEMENTS

The authors thank Agri Ibrahim Cecen University for financial support of the study (Project no: MYO-20-003).

CONFLICTS OF INTEREST

No conflict of interest was declared by the authors.

REFERENCES

[1] Anta, J. A., Guillén, E., Tena-Zaera, R., “ZnO-based dye-sensitized solar cells”, The Journal of Physical Chemistry C, 116(21), 11413-11425, (2012).

EARLY VIEW

[2] Ghosh, S., Saha, M., Paul, S., De, S. K., "Shape controlled plasmonic Sn doped CdO colloidal nanocrystals: a synthetic route to maximize the figure of merit of transparent conducting oxide. Small", 13 (7), 1602469, (2017).

[3] El Radaf, I. M., Hameed, T. A., Dahy, T. M., "Synthesis, structural, linear and nonlinear optical properties of chromium doped SnO_2 thin films", Ceramics International, 45 (3), 3072-3080, (2019).

[4] Pal, D., Singhal, J., Mathur, A., Singh, A., Dutta, S., Zollner, S.,Chattopadhyay, S., "Effect of substrates and thickness on optical properties in atomic layer deposition grown ZnO thin films", Applied Surface Science, 421, 341-348, (2017).

[5] Ganesh, V., Arif, M., Manthrammel, M. A., Shkir, M., Singh, A., AlFaify, S., "Effect of La doping on key characteristics of SnO_2 thin films facilely fabricated by spin coating technique", Optical Materials, 94, 277-285, (2019).

[6] Benkara, S., Ghamri, H., Rechem, D., Zaabat, M., "Effect of experimental parameters and (Fe, Ni) doping on the structural, morphological, and optical properties of sol–gel dip-coated SnO_2 films", Journal of Materials Research, 32 (8), 1594-1602, (2017).

[7] Suthakaran, S., Dhanapandian, S., Krishnakumar, N., Ponpandian, N., "Hydrothermal synthesis of surfactant assisted Zn doped SnO_2 nanoparticles with enhanced photocatalytic performance and energy storage performance", Journal of Physics and Chemistry of Solids, 141, 109407, (2020).

[8] Houaidji, N., Ajili, M., Chouial, B., Kamoun, N. T.,Kamli, K., Khadraoui, A., Hadef, Z., Zaidi, B., Hadjoudja, B., "Study of Mn Doping on the Structural, Optoelectronic and Photoluminescence Properties of F-Doped SnO_2 Sprayed Thin Films for Optoelectronic Applications", In Journal of Nano Research, 65, 13-26, (2020).

[9] Ashtari, P., Pourghahramani, P., "Hydrometallurgical recycling of cobalt from zinc plants residue", Journal of Material Cycles and Waste Management, 20(1): 155-166, (2018).

[10] Kim, H., Auyeung, R. C. Y., Piqué, A., "Transparent conducting F-doped SnO_2 thin films grown by pulsed laser deposition", Thin Solid Films, 516 (15): 5052-5056, (2008).

[11] Yu, S., Li, L., Sun, Z., Zheng, H., Dong, H., Xu, D., Zhang, W., "Characteristics of Transparent Conducting W-Doped SnO_2 Thin Films Prepared by Using the Magnetron Sputtering Method", Journal of the American Ceramic Society, 98 (4): 1121-1127, (2015).

[12] Okuno, T., Oshima, T., Lee, S. D., Fujita, S., "Growth of SnO_2 crystalline thin films by mist chemical vapour deposition method", Physica Status Solidi C, 8(2): 540-542, (2011).

[13] İskenderoğlu, Demet, Harun Güney, and Muhammed Emin Güldüren. "Chromium–An effective dopant for engineering the structural and the optical properties of CdO nanostructures grown by SILAR method", Optical Materials, 115: 111067, (2021).

[14] Liu, J., Liu, X., Zhai, Z., Jin, G., Jiang, Q., Zhao, Y., Luo, C., Quan, L., "Evaluation of depletion layer width and gas-sensing properties of antimony-doped tin oxide thin film sensors", Sensors and Actuators B: Chemical, 220: 1354-1360, (2015).

[15] Batzill, M., Burst, J. M., Diebold, U., "Pure and cobalt-doped SnO_2 (101) films grown by molecular beam epitaxy on Al2O3", Thin Solid Films, 484(1-2): 132-139, (2005).

[16] Velusamy, P., Babu, R. R., Ramamurthi, K., Elangovan, E., Viegas, J., "Effect of La doping on the structural, optical and electrical properties of spray pyrolytically deposited CdO thin films", Journal of Alloys and Compounds, 708, 804-812, (2017).

EARLY VIEW

[17] Pelaez, M., Nolan, N. T., Pillai, S. C., Seery, M. K., Falaras, P., Kontos, A. G.,Hamilton, J.,Byrne, J.,O'Shea, K., Entezari, M.,Dionysiou, D. D., "A review on the visible light active titanium dioxide photocatalysts for environmental applications", Applied Catalysis B: Environmental, 125: 331-349, (2012).

[18] Takagahara, T., Takeda, K., "Theory of the quantum confinement effect on excitons in quantum dots of indirect-gap materials", Physical Review B, 46(23): 15578, (1992).

[19] Li, Y., Yin, W., Deng, R., Chen, R., Chen, J., Yan, Q., Sun, H., Wei, S., Wu, T., "Realizing a SnO_2-based ultraviolet light-emitting diode via breaking the dipole-forbidden rule", NPG Asia Materials, 4 (11): e30-e30, (2012).

[20] Entradas, T., Cabrita, J. F., Dalui, S., Nunes, M. R., Monteiro, O. C., Silvestre, A. J., "Synthesis of sub-5 nm Co-doped SnO_2 nanoparticles and their structural, microstructural, optical and photocatalytic properties", Materials Chemistry and Physics, 147 (3): 563-571, (2014).

[21] Chun-Ming, L., Li-Mei, F., Xiao-Tao, Z., Wei-Lie, Z., "The influence of nickel dopant on the microstructure and optical properties of SnO_2 nano-powders", Chinese Physics, 16 (1): 95, (2007).

[22] Turgut, G., Keskenler, E. F., Aydın, S., Sönmez, E., Doğan, S., Düzgün, B., Ertuğrul, M., "Effect of Nb doping on structural, electrical and optical properties of spray deposited SnO_2 thin films", Superlattices and Microstructures, 56: 107-116, (2013).

[23] Dugan, S., Koç, M.M. and Coşkun, B., "Structural, electrical and optical characterization of Mn doped CdO photodiodes", Journal of Molecular Structure, 1202, 127235, (2020).

[24] Yetim, N.K., Aslan, N., Sarıoğlu, A., Sarı, N. and Koç, M.M., "Structural, electrochemical and optical properties of hydrothermally synthesized transition metal oxide (Co_3O_4, NiO, CuO) nanoflowers", Journal of Materials Science: Materials in Electronics, 31(15), 12238-12248, (2020).

[25] İlhan, M., Koç, M.M., Coşkun, B. and Yakuphanoğlu, F., "Optical, Electrical and Photo responsive Properties of Cu_2NiSnS_4 Solar Detectors", Journal of Electronic Materials, 49, 4457-4465, (2020).

[26] Uysal, B. Ö., Arier, Ü. Ö. A., "Structural and optical properties of SnO_2 nano films by spin-coating method", Applied Surface Science, 350: 74-78, (2015).

[27] Hwang, J. D., Ho, T. H., "Effects of oxygen content on the structural, optical, and electrical properties of NiO films fabricated by radio-frequency magnetron sputtering", Materials Science in Semiconductor Processing, 71: 396-400, (2017).

[28] Luo, S., Fan, J., Liu, W., Zhang, M., Song, Z., Lin, C., Wu, X., Chu, P. K., "Synthesis and low-temperature photoluminescence properties of SnO_2 nanowires and nanobelts", Nanotechnology, 17(6): 1695, (2006).

[29] Deepa, S., Kumari, K. P., Thomas, B. Contribution of oxygen-vacancy defect-types in enhanced CO2 sensing of nanoparticulate Zn-doped SnO_2 films", Ceramics International, 43(18): 17128-17141, (2017).

[30] Sangeetha, P., Sasirekha, V., Ramakrishnan, V., "Micro-Raman investigation of tin dioxide nanostructured material based on annealing effect", Journal of Raman Spectroscopy, 42(8): 1634-1639, (2011).

EARLY VIEW